Supporting information

The Nature of Oxygen Vacancy and Spinel Phase Integration on Both Anionic and Cationic Redox in Li-rich Cathode Material

*Qingyuan Li[a], De Ning[b], Dong Zhou[b], Ke An[c], Deniz Wong[b], Lijuan Zhang[d], Zhenhua Chen[d], Götz Schuck[b], Christian Schulz[b], Zijian Xu[d], Gerhard Schumacher[b] and Xiangfeng Liu[a]**

[a] Center of Materials Science and Optoelectronics Engineering, College of Materials Science and Optoelectronic Technology, University of Chinese Academy of Sciences, Beijing 100049, P. R. China

[b] Helmholtz-Center Berlin for Materials and Energy, Hahn-Meitner-Platz 1, Berlin 14109, Germany

[c] Neutron Scattering Division, Oak Ridge National Laboratory, Oak Ridge, Tennessee, 37830, USA

[d] Shanghai Synchrotron Radiation Facility, Shanghai Institute of Applied Physics, Chinese Academy of Sciences, Shanghai 201204, P. R. China

*E-mail: liuxf@ucas.ac.cn

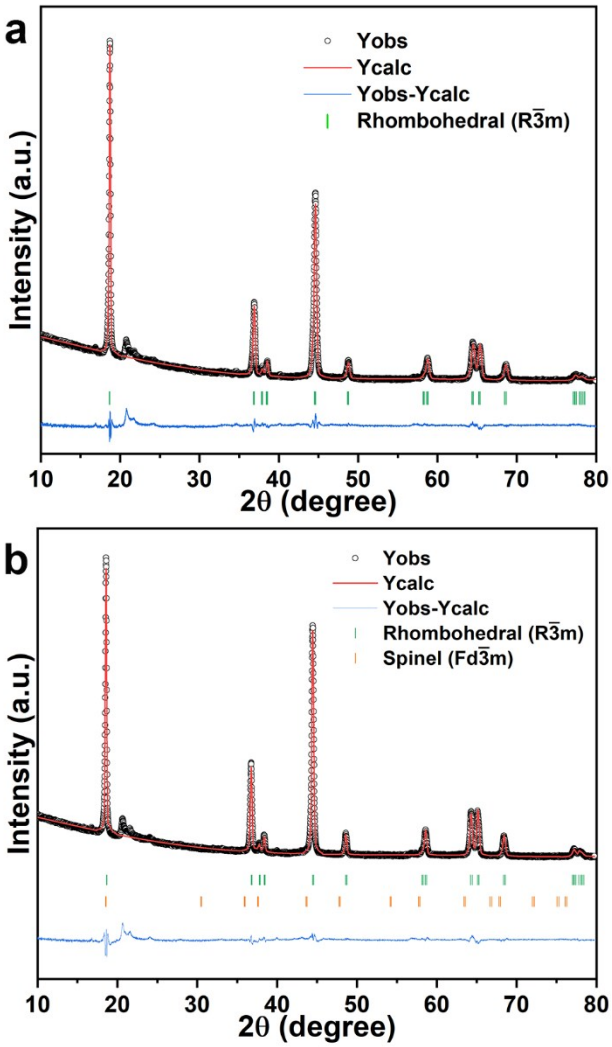

Figure S1. The XRD Rietveld refined patterns of (a) pristine material and (b) OV sample.

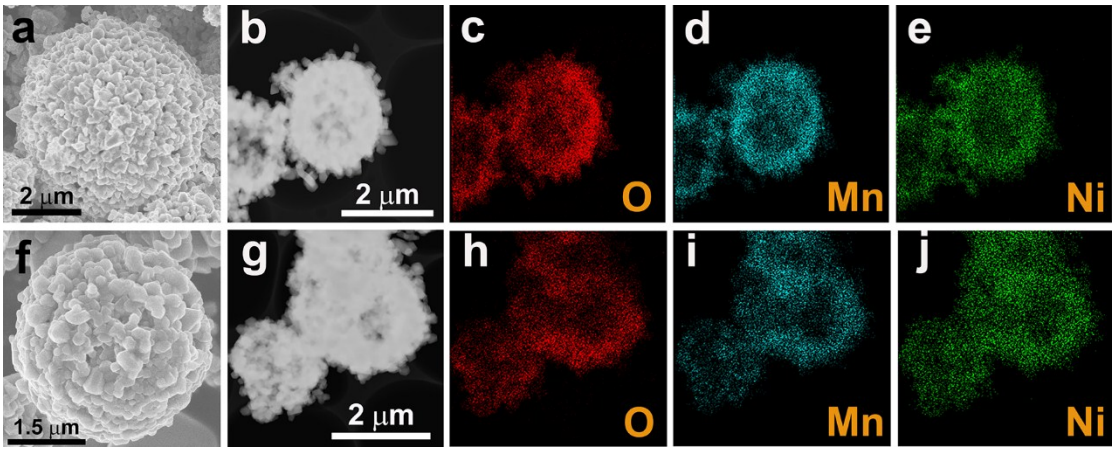

Figure S2. (a and f) The SEM images of pristine and OV sample, respectively. (b-e and g-j) The STEM images and O, Mn and Ni EDS mappings of pristine and OV sample, respectively.

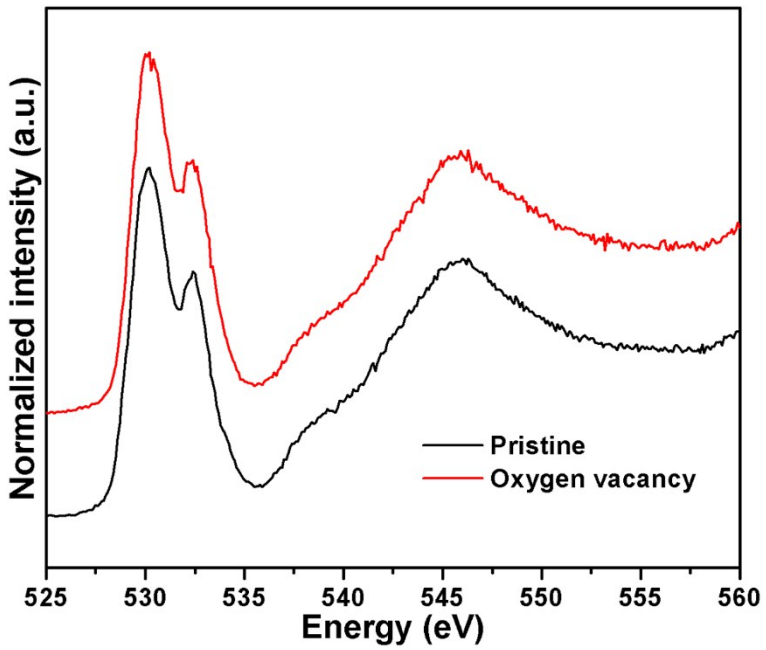

Figure S3. O K-edge pattern of pristine and OV samples with FY mode.

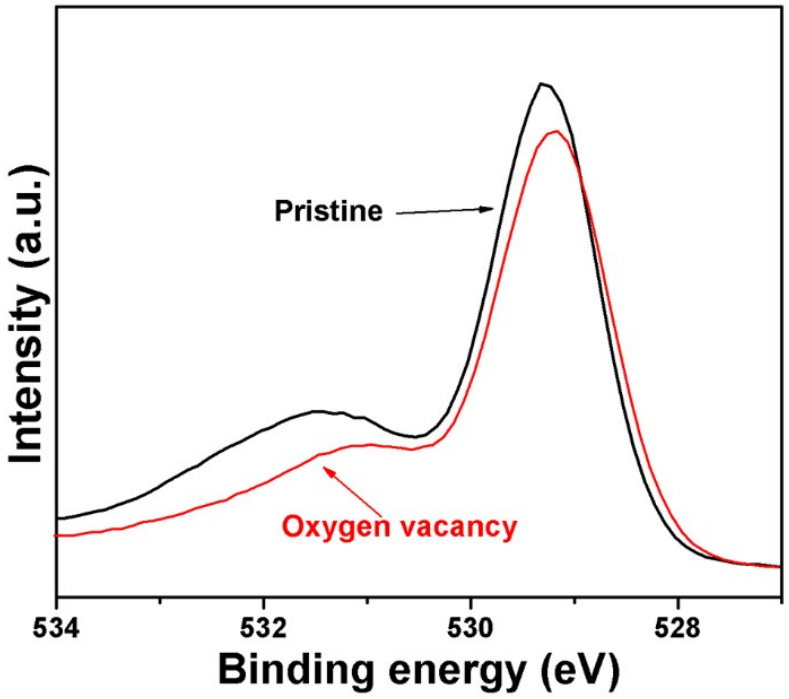

Figure S4. O 1s XPS spectra of pristine and OV materials.

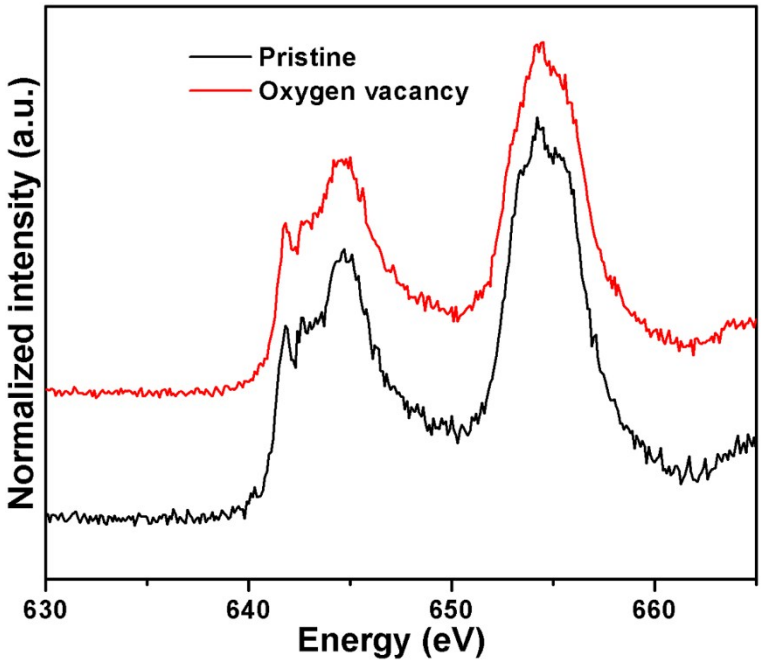

Figure S5. Mn L-edge of pristine and OV samples with FY mode.

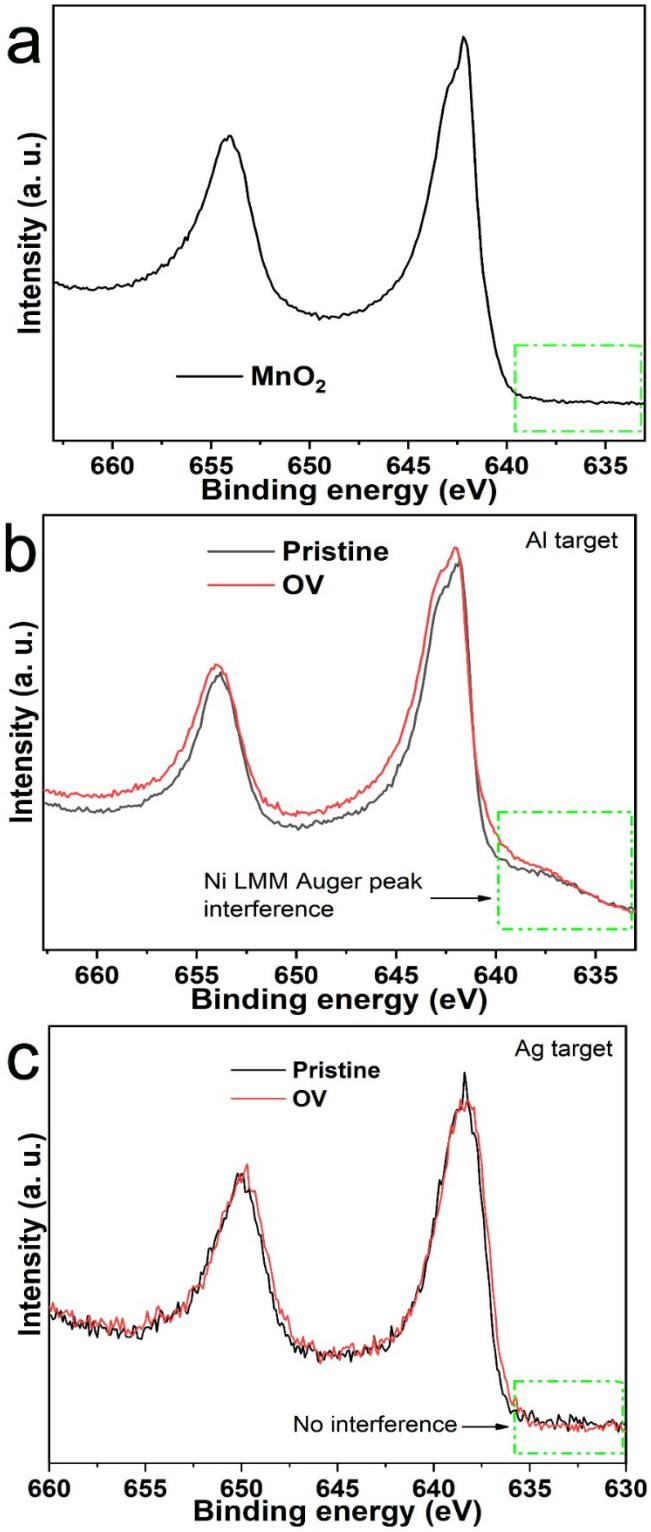

Figure S6. (a) Mn 2p XPS spectrum of pure MnO_2, (b and c) XPS spectra of Mn 2p tested with an Al and Ag target, respectively, in both samples. As the rectangle boxes show, the Ni LMM auger peak can be eliminated completely by the measuring with an Ag target.

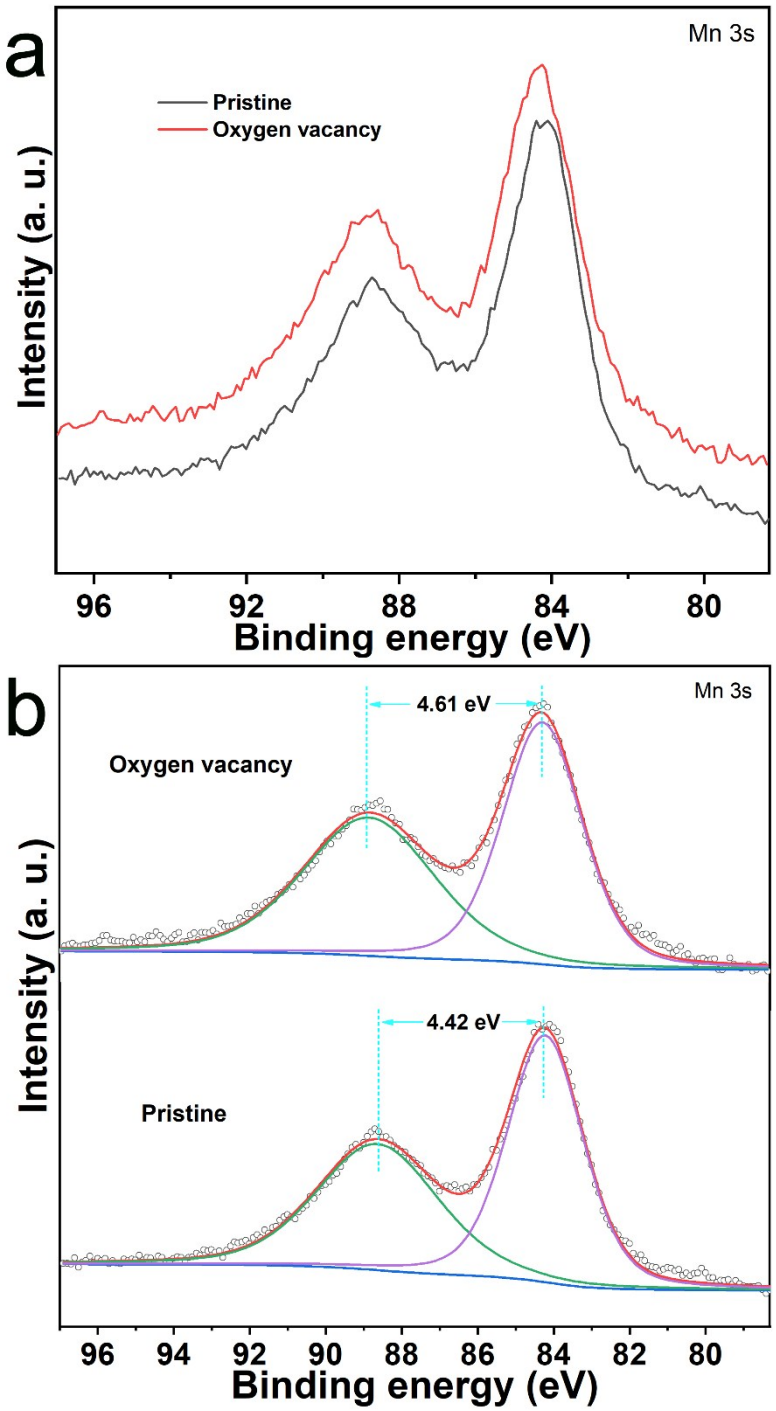

Figure S7. (a) XPS spectra of Mn 3s and (b) the corresponding fitting peaks and splitting energy in both the samples.

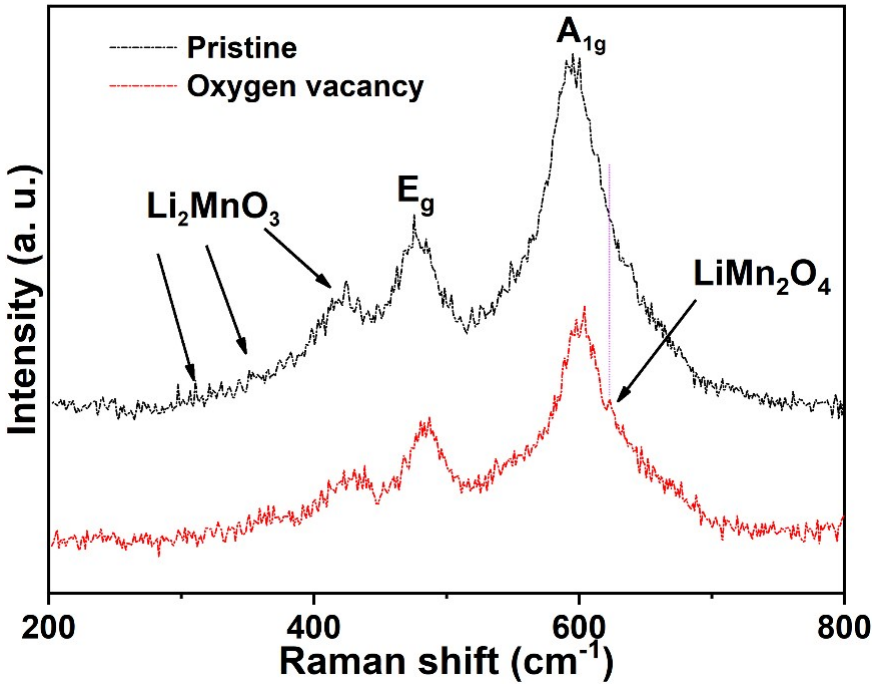

Figure S8. Raman spectra of pristine and OV samples. The two broad peaks at approximately 490 and 602 cm^{-1} can be ascribed to the E_g and A_{1g} mode of $R\bar{3}m$ layer structure. The peaks of Li_2MnO_3 can be found between 320 and 440 cm^{-1}.[1-2] The Raman band of $LiMn_2O_4$ can be observed at approximately 625 cm^{-1}, which can be attributed to the A_{1g} species in the spinel $LiMn_2O_4$ structure.[3]

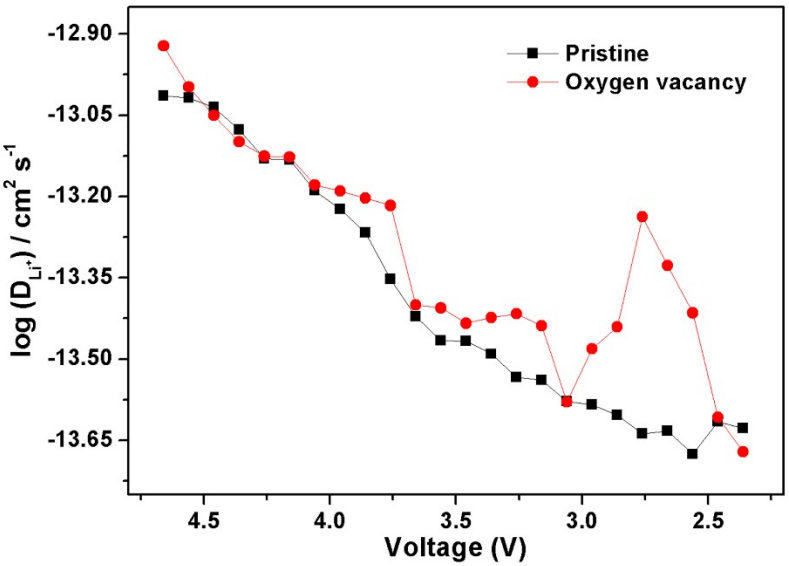

Figure S9. Relationship of the transition current (I) with the titration time (t) at different charge-discharge states for pristine and OV samples. The corresponding maximum coefficient of pristine and OV sample is 9.68 $\times 10^{-14}$ and 1.20 $\times 10^{-13}$ cm^2 s^{-1}, respectively during the discharge process.

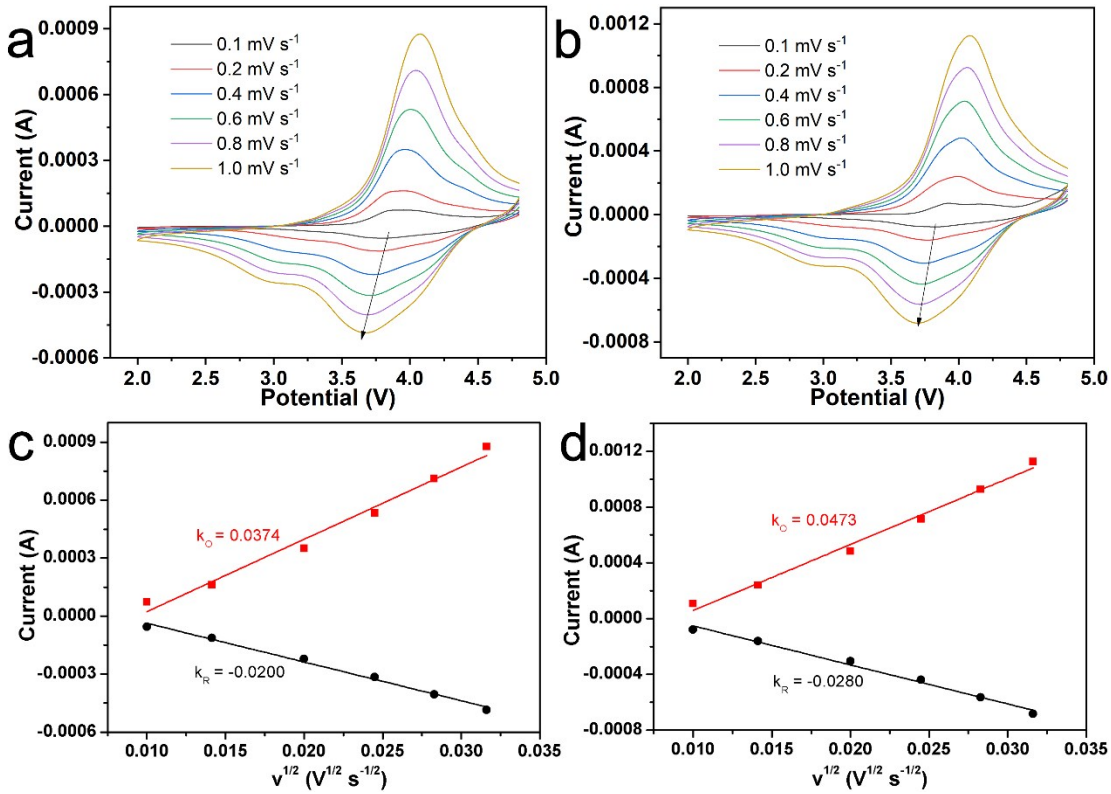

Figure S10. CV curves of pristine (a) and OV samples (b) at different scan rates; (c and d) representing the relationships of the peak current (I_P) and the square root of scan rate ($v^{1/2}$). The Li^+ diffusion coefficient can be calculated by the Randle-Sevcik equation:

$$I_p = (2.69 \times 10^5) n^{3/2} A D_{Li}^{1/2} v^{1/2} C_{Li}$$

where I_p is the peak current; n is the charge transfer number; A is the surface area of the electrode; v is the scan rate and C_{Li} is the bulk concentration of Li^+ in the materials. The lithium ions diffusion coefficients of pristine and OV samples are 8.82×10^{-14} cm^2 s^{-1} and 1.4×10^{-13} cm^2 s^{-1}, respectively, for oxidation process. The values of the two samples are 2.53×10^{-14} cm^2 s^{-1} and 4.93×10^{-14} cm^2 s^{-1}, respectively, during reduction process.

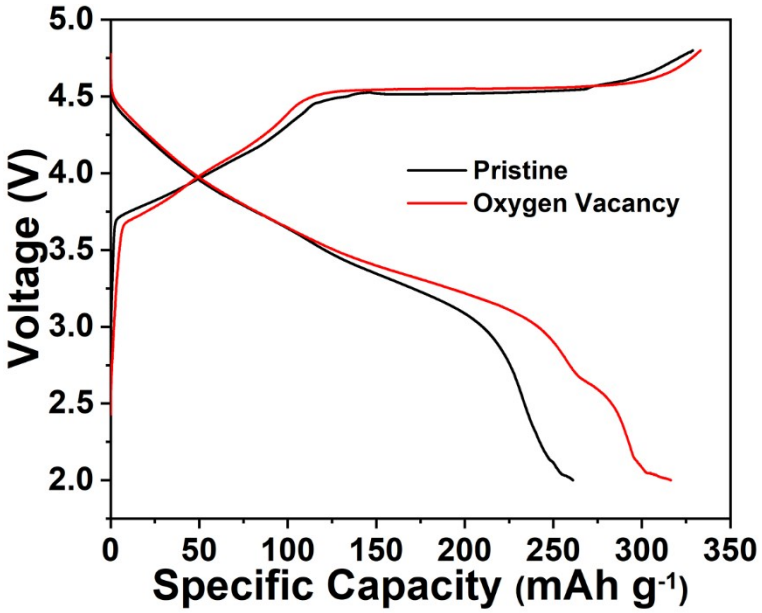

Figure S11. The first charge-discharge profiles of pristine and OV samples at 0.05 C.

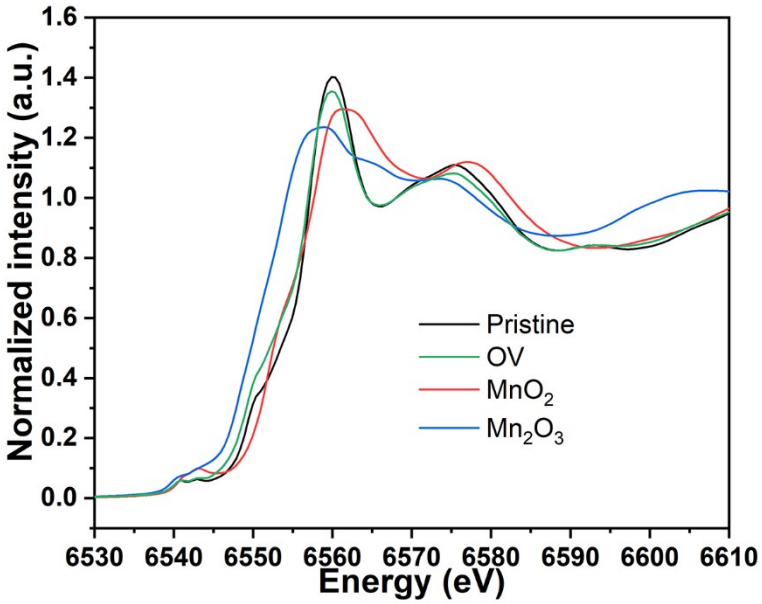

Figure S12. Mn K-edge XANES spectra of uncharged pristine and OV samples. For comparison the reference compounds MnO_2 and Mn_2O_3 are added.

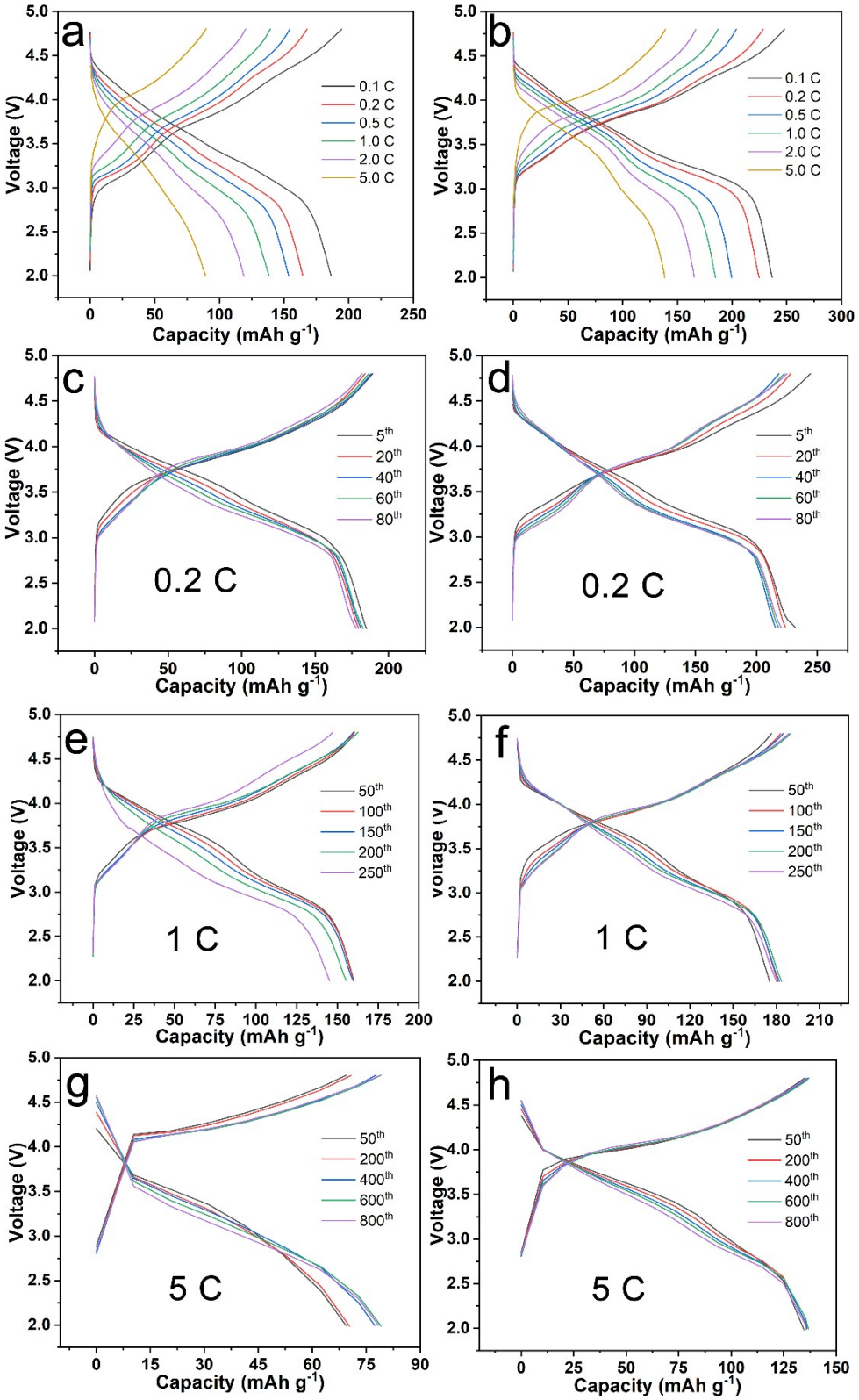

Figure S13. Voltage profiles of different cycles and different current density. The patterns of a, c, e and g represent the pristine sample, and those of b, d, f and h show the OV sample.

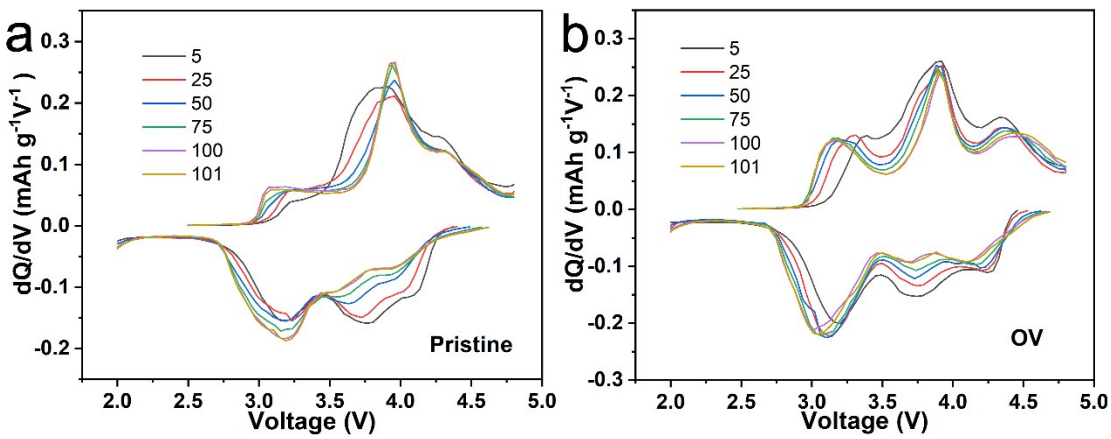

Figure S14. dQ/dV curves of (a) pristine and (b) OV samples at different cycles at 0.2C.

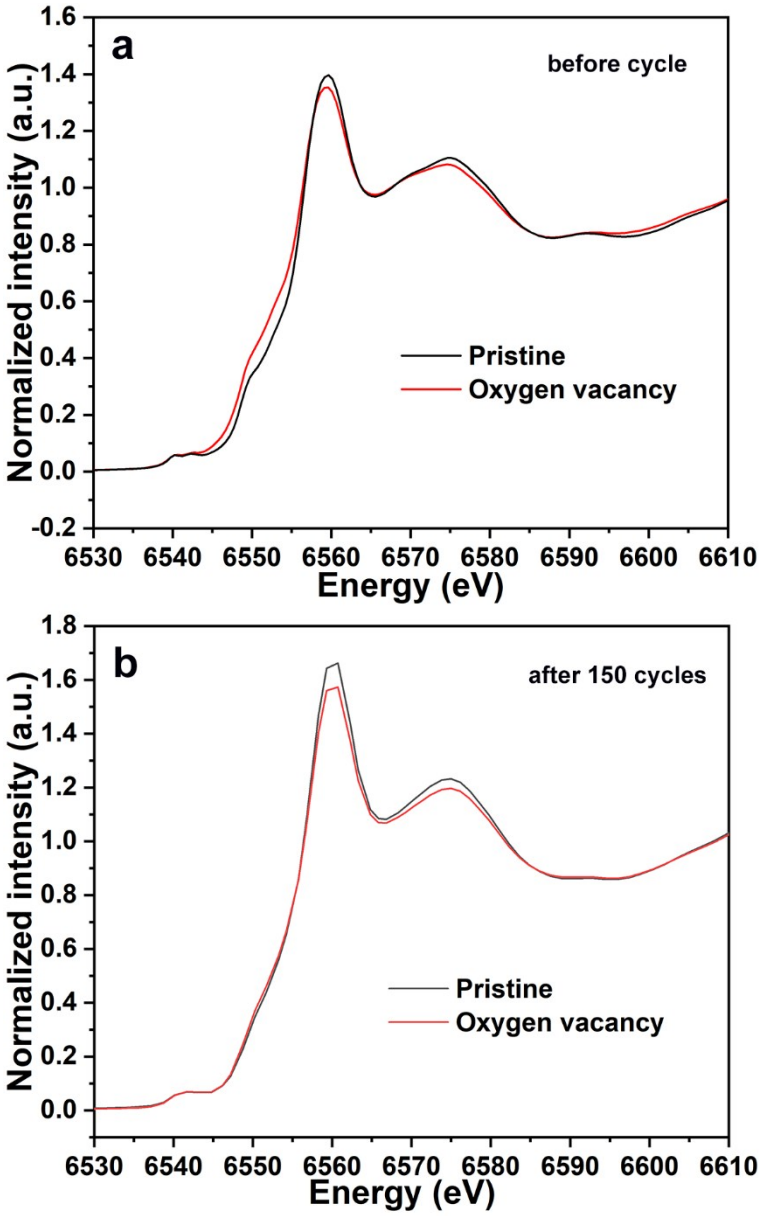

Figure S15. Mn K-edge XANES spectra of (a) before cycle and (b) after 150 cycles at the current density of 1 C. The height of white line of pristine is approximately 3% higher than that of OV sample before cycle. For comparison, the difference widened to 9% after 150 cycles, which indicates there is a larger MnO_6 octahedral distortion in the OV sample.

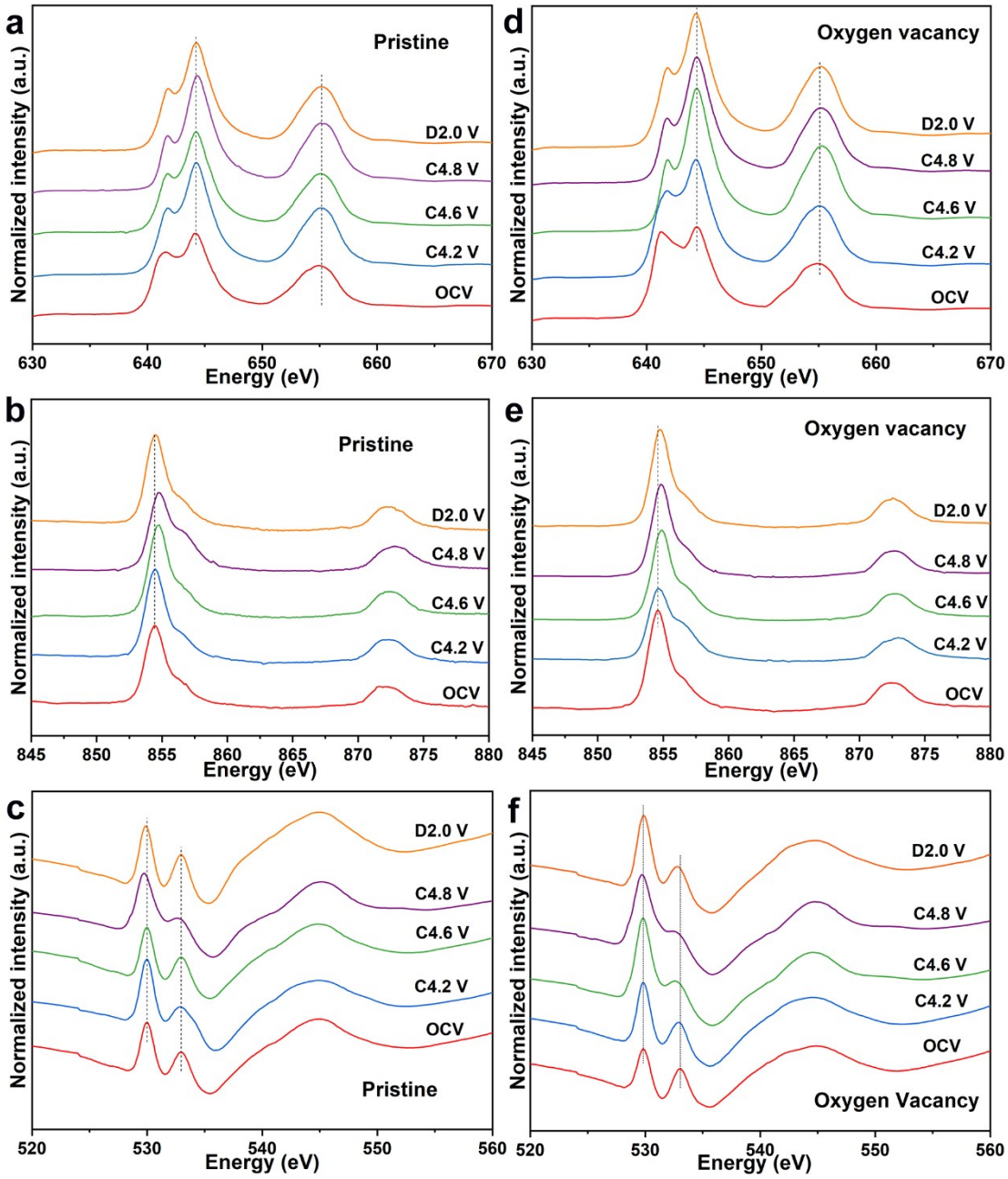

Figure S16. Ex situ soft XAS spectra of (a-c) pristine and (d-f) OV sample in TEY mode. (a and d) Mn L-edge, (b and e) Ni L-edge, (c and f) O K-edge.

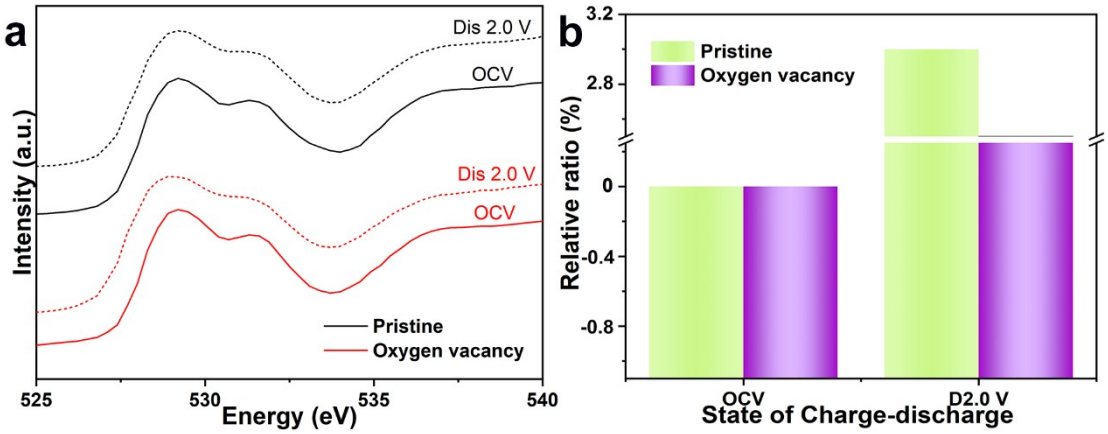

Figure S17. (a) O K-edge XAS spectra at different charge and discharge states in FY mode. (b) A comparison of the relative integrated intensity between 525 and 534 eV for pristine and OV sample.

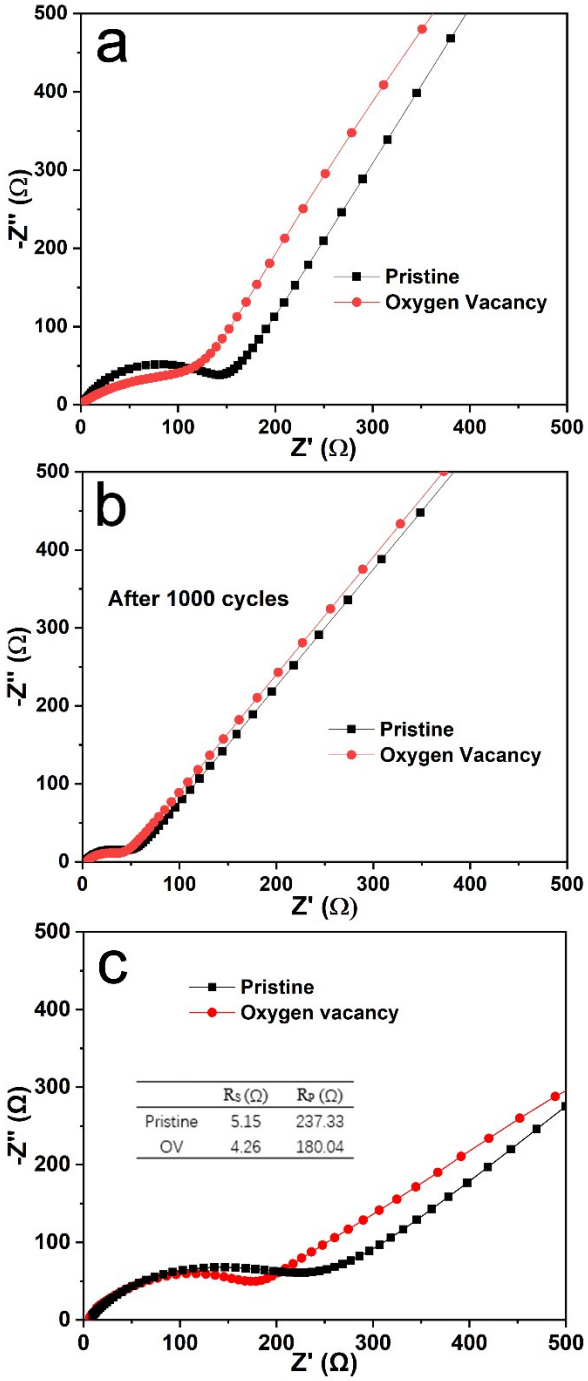

Figure S18. EIS spectra of pristine and OV materials. (a) Before cycling, (b) after 1000 cycles at 5 C and (c) after 10 cycles at 0.1 C. As the inset shows, Rs and Rp represent the internal resistance of the battery and the resistance of SEI film, respectively.

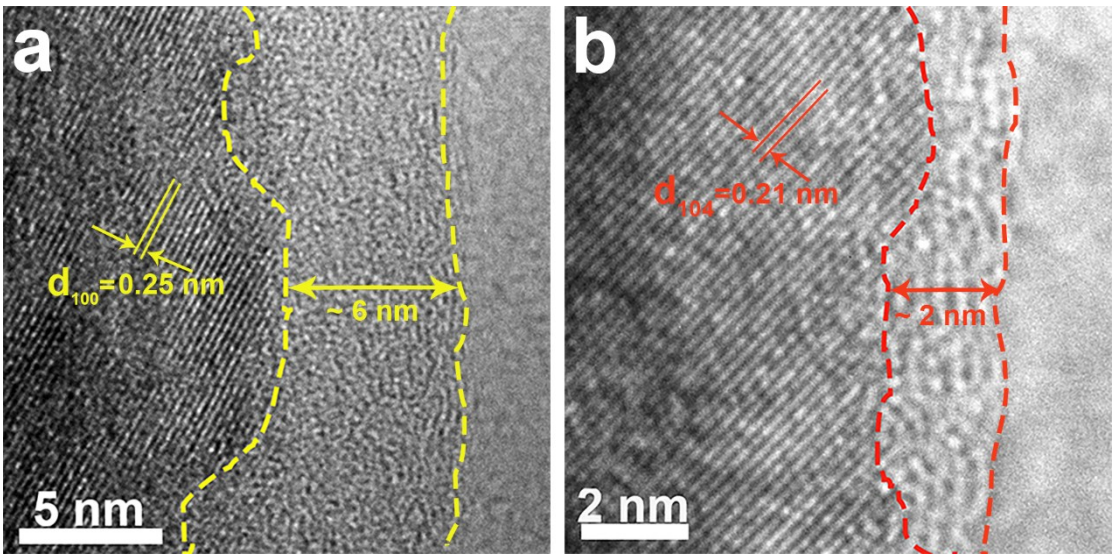

Figure S19. HRTEM images of (a) pristine and (b) OV sample after 250 cycles at 1 C.

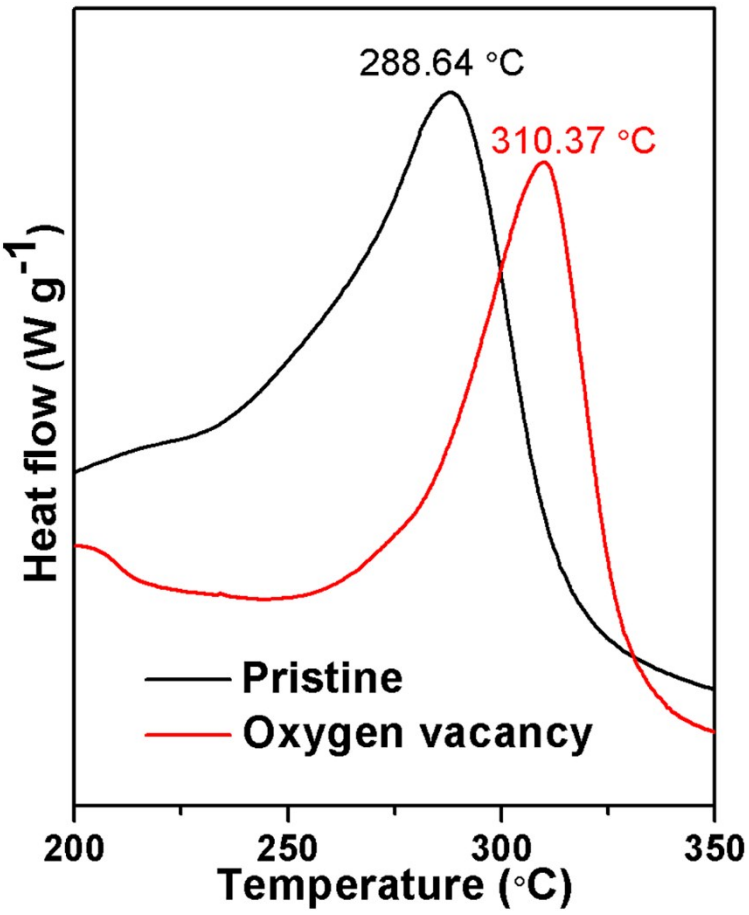

Figure S20. DSC patterns of the pristine and OV samples charged to 4.8 V.

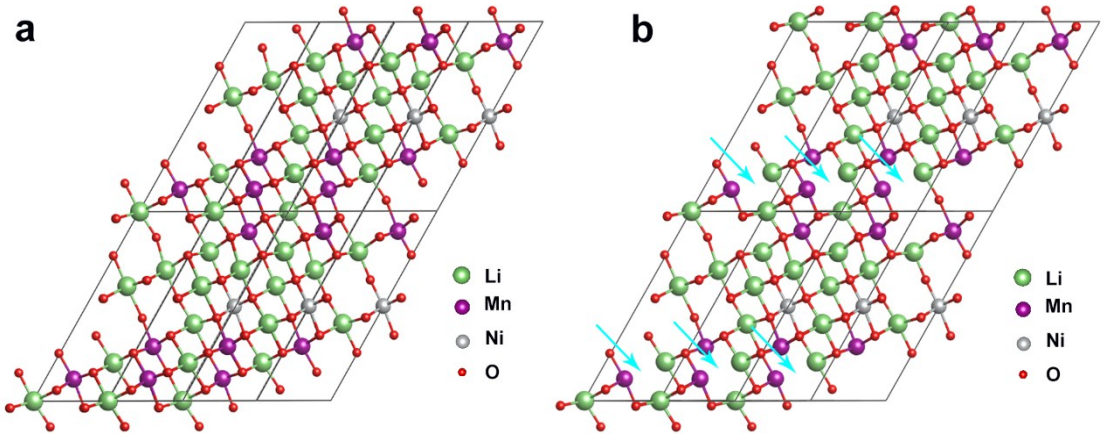

Figure S21. The crystal structure model of (a) pristine and (b) OV sample for DFT calculation. The cyan arrows show the position of oxygen atoms.

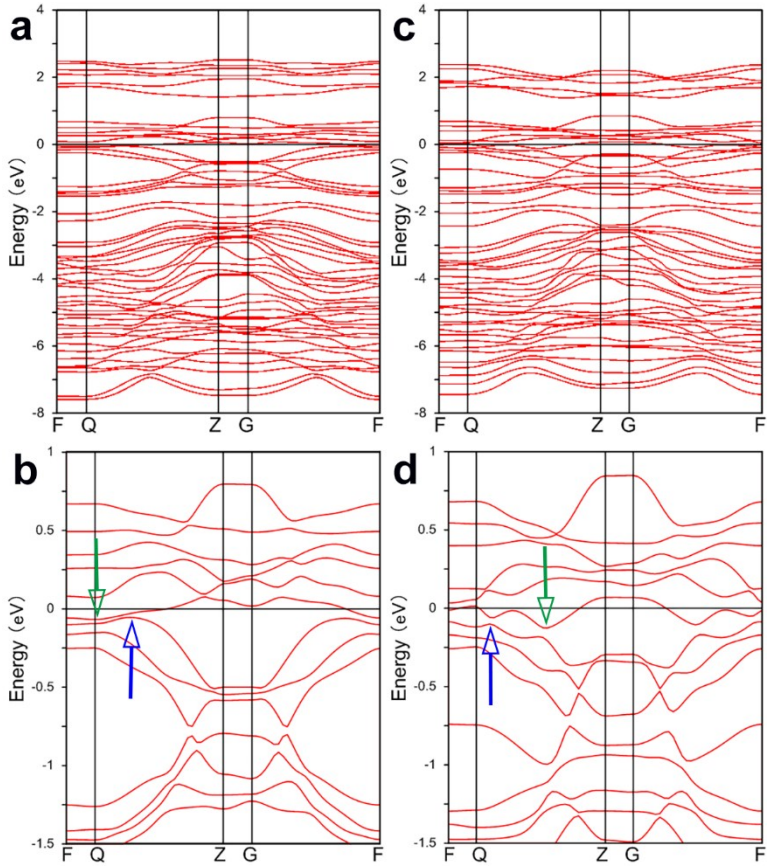

Figure S22. Calculated energy band structures of (a and b) pristine and (c and d) OV sample. The (b) and (d) are from the enlarged (a) and (c), repectively.

Table S1. ICP-MS results of pristine and OV samples

Samples	Norminal ratio			Experimental ratio		
	Li	Mn	Ni	Li	Mn	Ni
Pristine	1.2	0.6	0.2	1.2	0.6407	0.2190
OV				1.2	0.6325	0.2046

Table S2. Site Occupation of Atoms in Pristine Material and OV from Rietveld Refinement of the Neutron Diffraction Patterns.

Sample	Atom	Site	x	y	z	Occupation
Pristine	Li1	3a	0	0	0	0.981(5)
	Ni1	3a	0	0	0	0.019(5)
	Mn	3b	0	0	0.5	0.600
	Ni2	3b	0	0	0.5	0.181(5)
	Li2	3b	0	0	0.5	0.219(6)
	O	6c	0	0	0.24095(5)	1.000(4)
OV	Li1	3a	0	0	0	0.971(2)
	Ni1	3a	0	0	0	0.029(2)
	Mn	3b	0	0	0.5	0.600
	Ni2	3b	0	0	0.5	0.171(2)
	Li2	3b	0	0	0.5	0.229(2)
	O	6c	0	0	0.24136(6)	0.967(3)

Table S3. Comparison of the electrochemical performance of free-cobalt Li1.2Ni0.2Mn0.6O2 and its modified samples.*

Materials	Current density (mA/g)	No. of cycles	Remaining capacity	References
OV-LMNO	50	100	219	This Work
	250	250	183	
	1250	1000	131	
spinel-layered $Li_{1.2}Mn_{0.75}Ni_{0.25}O_{2+\delta}$	19	50	<270	4
Nano-Crystalline $Li_{1.2}Mn_{0.6}Ni_{0.2}O_2$	20	50	179	5
$LaNiO_3$@LMNO(1.5 wt%)	25	200	204.1	6
LMNO – 900℃-24h	25	50	180	7
LMNO	25	50	260	8
Hierarchically porous $Li_{1.2}Mn_{0.6}Ni_{0.2}O_2$	30	30	200	9
FD-LMNO	50	100	232	10
$Li_{1.2}Mn_{0.57}Ni_{0.2}O_2$	100	100	157.10	11
$Li_{1.2}Mn_{0.6-x}Ni_{0.2}Y_xO_2$ (x＝0.03)	200	40	184.5	12
$Li_\delta V_2O_5$@LMNO	200	50	181	13
SC-LCM	200	50	142.74	14
PLMNO	200	200	197	15
Syn-Li_2ZrO_3@LMNO	250	100	162	16
Fe doped $Li_{1.2}Mn_{0.6-x/2}Ni_{0.2-x/2}Fe_xO_2$ (x≤0.1)	250	150	165	17
$Li_{1.2}Mn_{0.6}Ni_{0.2}O_2$ microspheres	250	100	183.3	18
Hierarchical $Li_{1.2}Ni_{0.2}Mn_{0.6}O_2$ Nanoplates	250	60	216.2	19
1%CeO_2@LMNO	300	200	171	20
Ti-modified layered–spinel $Li_{1.2}Mn_{0.75}Ni_{0.25}O_{2+\delta}$	308	200	145	21
Organic carbon gel for LMNO	400	150	183.7	22
$Li_{1.17}Ni_{0.17}Mn_{0.67}O_2$	0.2C	50	207	23
Li1.2Ni0.18Mn0.58Al0.04O2	0.2C	50	≈220	24
Boron-doped $Li_{1.2}Mn_{0.6}Ni_{0.2}O_2$	1C	275	132.1	25
Monodisperse $Li_{1.2}Mn_{0.6}Ni_{0.2}O_2$	1C	50	168	26
1% Fe doping LMNO	1C	200	≈155	27

Reference

1 J. Zhao, R. Huang, W. Gao, J.-M. Zuo, X. F. Zhang, S. T. Misture, Y. Chen, J. V. Lockard, B. Zhang, S. Guo, M. R. Khoshi, K. Dooley, H. He, Y. Wang, *Adv. Energy Mater.* 2015, **5**, 1401937.

2 R. Yu, X. Zhang, T. Liu, L. Yang, L. Liu, Y. Wang, X. Wang, H. Shu, X. Yang, *ACS Appl. Mater. Interfaces* 2017, **9**, 41210-41223.
3 C. V. Ramana, M. Massot, C. M. Julien, *Surf. Interface Anal.* 2005, **37**, 412-416.
4. N. H. Vu, P. Arunkumar, J. C. Im, D. T. Ngo, H. T. T. Le, C.-J. Park and W. Bin Im, *J. Mater. Chem. A*, 2017, **5**, 15730-15742.
5. X. He, J. Wang, L. Wang and J. Li, *Materials*, 2016, **9**, 661.
6. F. Wu, Q. Li, L. Bao, Y. Zheng, Y. Lu, Y. Su, J. Wang, S. Chen, R. Chen and J. Tian, *Electrochim. Acta*, 2018, **260**, 986-993.
7. C.-C. Wang, K. A. Jarvis, P. J. Ferreira and A. Manthiram, *Chem. Mater.*, 2013, **25**, 3267-3275.
8. X. Li, Y. Qiao, S. Guo, Z. Xu, H. Zhu, X. Zhang, Y. Yuan, P. He, M. Ishida and H. Zhou, *Adv. Mater.*, 2018, **30**, e1705197.
9. S. Duraisamy, T. R. Penki and M. Nookala, *New J. Chem.*, 2016, **40**, 1312-1322.
10. P. Yang, H. Li, X. Wei, S. Zhang and Y. Xing, *Electrochim. Acta*, 2018, **271**, 276-283.
11. Z. Tai, X. Li, W. Zhu, M. Shi, Y. Xin, S. Guo, Y. Wu, Y. Chen and Y. Liu, *J. Colloid Interface Sci.*, 2020, **570**, 264-272.
12. N. Li, R. An, Y. Su, F. Wu, L. Bao, L. Chen, Y. Zheng, H. Shou and S. Chen, *Journal of Materials Chemistry A*, 2013, **1**, 9760-9767.
13. S.-X. Liao, C.-H. Shen, Y.-J. Zhong, W.-H. Yan, X.-X. Shi, S.-S. Pei, X. Guo, B.-H. Zhong, X.-L. Wang and H. Liu, *Rsc Advances*, 2014, **4**, 56273-56278.
14. L. Wang, Z.-B. Wang, F.-D. Yu, B.-S. Liu, Y. Zhang and Y.-X. Zhou, *Ceram. Int.*, 2016, **42**, 14818-14825.
15. S. Qiu, T. Fang, Y. Zhu, J. Hua, H. Chu, Y. Zou, J.-L. Zeng, F. Xu and L. Sun, *J. Alloys Compd.*, 2019, **790**, 863-870.
16. J. Zhang, H. Zhang, R. Gao, Z. Li, Z. Hu and X. Liu, *Phys. Chem. Chem. Phys.*, 2016, **18**, 13322-13331.
17. X. Liu, T. Huang and A. Yu, *Electrochim. Acta*, 2014, **133**, 555-563.
18. J. Meng, S. Zhang, X. Wei, P. Yang, S. Wang, J. Wang, H. Li, Y. Xing and G. Liu, *Rsc Advances*, 2015, **5**, 81565-81572.
19. L. Chen, Y. Su, S. Chen, N. Li, L. Bao, W. Li, Z. Wang, M. Wang and F. Wu, *Adv. Mater.*, 2014, **26**, 6756-6760.
20. J. Wu, C. Han, H. Wu, H. Liu, Y. Zhang and C. Lu, *Ionics*, 2019, **25**, 3031-3040.
21. N. H. Vu, J. C. Im, S. Unithrattil and W. B. Im, *J. Mater. Chem. A*, 2018, **6**, 2200-2211.
22. E. Wang, C. Shao, S. Qiu, H. Chu, Y. Zou, C. Xiang, F. Xu and L. Sun, *Rsc Advances*, 2017, **7**, 1561-1566.
23. T. Sarkar, K. R. Prakasha, M. D. Bharadwaj and A. S. Prakash, *J. Phys. Chem. C*, 2017, **121**, 20591-20596.
24. J. Chen, Y. Wang, N. Zhao and Z.-Q. Liu, *Scr. Mater.*, 2019, **171**, 47-51.
25. D. Uzun, *Solid State Ionics*, 2015, **281**, 73-81.
26. F. Cheng, Y. Xin, J. Chen, L. Lu, X. Zhang and H. Zhou, *Journal of Materials Chemistry A*, 2013, **1**, 5301-5308.
27. D. Zhang, Z. Li, G. Li, M. Zhang and Y. Yan, *ChemistrySelect*, 2019, **4**, 13058-13063.